Batteries & Supercaps

Review
doi.org/10.1002/batt.202300321

Chemistry Europe
European Chemical Societies Publishing

www.batteries-supercaps.org

Electro-Chemo-Mechanical Failure Mechanisms of Solid-State Electrolytes

Quan Wu,[a, c] Shizhao Xiong,[c] Fujun Li,*[a, b] and Aleksandar Matic*[c]

Solid-state lithium-metal batteries (SSLMBs) are considered as the next-generation energy storage systems due to their high theoretical energy density and safety. However, the practical deployment of SSLMBs has been impeded by the failure of solid-state electrolytes (SSEs) which is indicated by the increased impedance, elevated polarization, and capacity degradation. The failure is commonly a result of lithium (Li) dendrite growth and propagation, inactive Li generation, unstable interface formation, void and pore formation, and crack infiltration. The failure processes can be divided into electric failure, (electro)chemical failure, and mechanical failure based on the different mechanisms. The systematical understanding of SSEs failure is crucial for the development of SSEs. Therefore, this review comprehensively summarizes the details of the three SSEs failure to provide new insights for future studies, shedding light on the design of SSLMBs with high energy density, safety, and cycling stability.

1. Introduction

The current commercial lithium-ion batteries (LIBs) that utilize graphite anodes have almost reached their theoretical specific energy density (350 Wh kg^{-1}).[1] However, this energy density is insufficient to meet the practical requirements of long-range electric vehicles and smart grids.[2,3] Using Li metal instead of graphite in the cell has been considered as the natural next step in the development due to the high theoretical specific capacity of 3,861 mAh g^{-1} and low redox potential (−3.04 V vs. S.H.E.)[4] of Li. In the surge for high-energy-density, Li metal batteries (LMBs) will boost the energy density of state-of-art LIBs. However, uncontrolled formation of Li dendrites is a major problem encountered in LMBs, which may lead to capacity fade, short circuits and thermal runaway, posing a great hurdle for practical applications.[5]

Solid-state lithium-metal batteries (SSLMBs) have been proposed as a promising approach to considerably optimize the safety, cycling capability, and energy density of LMBs by replacing flammable liquid electrolyte with a solid-state electrolyte (SSE).[6,7] In general, SSEs can be divided into two major groups: inorganic solids including crystalline, glass, glass-ceramic and organic solid polymers. SSEs have higher thermal stability compared with traditional liquid electrolytes, which can largely prevent the electrolyte decomposition at high voltage, thermal runaway, and catastrophic failures of batteries, which essentially improves cyclability and safety.[8] Furthermore, the higher mechanical modulus (e.g., toughness or shear modulus, etc.) SSEs are expected to suppress the formation and propagation of Li dendrites further promoting safety and cycling stability.[9] In addition, a wider voltage window of some SSEs also enables the full utilization of the capacity of high-voltage cathodes, thus increasing the energy density of LMBs.[10,11] However, internal short circuits, increased impedance, and decayed capacities have severely impeded the practical application of SSLMBs, especially at high-power conditions which promote Li dendrite growth and crack propagation in SSEs.[12,13]

The underlying physical, mechanical, chemical, and electrochemical mechanisms behind cell failure are still not well understood and several advanced characterization methods have been employed to shed light on different phenomena. In situ auger electron microscopy (AEM)[14] can detect Li metal with high spatial resolution, and can probe pressure-dependent Li plating/stripping processes, providing information about the distribution and thickness of deposited Li. In situ scanning electron microscopy (SEM),[15] in situ high-resolution transmission electron microscopy (HRTEM),[16] and in-plane operando optical microscopy (OM),[17] have been applied to investigate crack permeation, which are directly related to the intrinsic mechanical properties, of SSEs, and dendrite formation, as well as porosity, surface roughness, defect distribution, or external/internal stress.[15] These methods provide 2D information whereas focused ion beam (FIB)-SEM[18] can be used to probe the morphology of cross-sections or even in 3D by consecutive slicing of the sample. In-situ synchrotron X-ray computed tomography (CT)[19] with high resolution can provide 3D images non-destructively facilitating the observation of the propagation of cracks and Li dendrites in the bulk of SSEs.[20] Atomic force microscopy (AFM) can detect the roughness and thickness of the surface of SSEs, which gives information about the 3D structure of formed interphases between SSE and Li anode.[21] Time-of-flight secondary ion mass spectrometry (ToF-SIMS) enables 3D elemental mapping, which helps to qualitatively investigate the composition of the interphase.[22]

Theoretical modeling and simulations can also provide an in-depth understanding of failure mechanisms and are not limited by the same constraints as experimental methods. For instance, Xiong et al. proposed a modified electro-chemo-mechanical failure model of SSEs, clarifying the failure mechanism rooted in the interplay of interfacial and internal defects via numerical simulation.[23] Zhao et al. present predictions about the current spot, voids formation, and development

[a] Q. Wu, Prof. F. Li
Renewable Energy Conversion and Storage Center (RECAST)
Key Laboratory of Advanced Energy Materials Chemistry (Ministry of Education)
College of Chemistry
Nankai University
300071, Tianjin (P. R. China)
E-mail: fujunli@nankai.edu.cn

[b] Prof. F. Li
Haihe Laboratory of Sustainable Chemical Transformations
300192, Tianjin (P. R. China)

[c] Q. Wu, Dr. S. Xiong, Prof. A. Matic
Department of Physics
Chalmers University of Technology
S41296, Göteborg (Sweden)
E-mail: matic@chalmers.se

based on the proposed electro-chemo-mechanical model.[24] These methods are based on a combination of experimental data and theoretical modeling and suggest pathways to understand failure in and for the design of SSEs.[25]

However, a systematic and detailed understanding of the failure mechanisms of SSEs, which is the prerequisite for designing SSEs with high performance, is still lacking. This review provides a comprehensive summary of the current understanding of failure mechanisms of SSEs, which can be classified into three types: electric failure, (electro)chemical failure, and mechanical failure. We cover the full chain of processes of SSEs failure, including initiation, development, consequence, and the most important factors behind the mechanisms. With this as a base direction for future research and guidelines for designing SSEs and SSLMBs with high performance can be established.

2. Electric Failure

2.1. Origin of electric failure

The occurrence of electric failure in SSLMBs is primarily due to three causes: internal short circuit, loss of electric contact, and the formation of inactive Li. The internal short circuit of the cell is triggered by the connection of the cathode and anode by Li dendrite growth and propagation when the applied current density exceeds the critical current density (CCD).[26] During charging, Li ions migrate through the electrolyte to the Li metal anode and form nuclei at the interface between the SSE and the Li metal anode. As the deposition progresses Li will deposit preferentially on these nuclei, resulting in the growth of Li filaments. These filaments grow to form dendrites, which can propagate through the SSE and potentially connect the cathode and anode causing a short circuit.[27] In addition, when the areal capacity reaches a critical value, unstable Li deposition and short circuits induced by Li dendrites can still occur even though the current density is lower than the CCD.[28] Therefore, not only the current density but also the areal capacity should be taken into account for the prevention of internal short circuits and electric failure.

2.2. Processes of Li deposition

To understand the Li-plating process in SSMBs one can build on the knowledge from Li deposition and dendrite nucleation and growth in liquid electrolytes. Firstly, Li nucleation occurs when the local overpotential exceeds the surface energy (Figure 1a).[29] The critical nucleation radius has been shown to be inversely dependent on the overpotential,[30] i.e., smaller nuclei are formed with increasing overpotential. Current density also influences the nucleation step, with larger nuclei, with whisker growth, at low current density, while at higher current density, smaller nuclei are formed (Figure 1c).[29] Sadd et al. investigated the microstructure evolution during Li deposition on a Cu substrate in liquid electrolytes via operando X-ray tomographic microscopy.[20] Needle-like, mossy-like, and integrated structures, form mechanically robust Li-dendrites. The results indicate that tall needle-like Li microstructures are formed at low current density, whereas at high current density, Li with shorter and denser mossy-like morphology is dominating (Figure 1d, e). The Young's modulus of the substrate, where the deposition occurs also affects the overpotential of nucleation and critical nucleation size. For a fixed current density, larger nuclei and fewer nucleation sites are formed on a substrate due to a higher sustained inner pressure (Figure 1b).[31] Thus, the nature of the substrate/interface, physical properties of the electrolyte, and current density influence the nucleation and growth toward the final morphology in liquid electrolytes. An

Quan Wu obtained her B. S. degree from China University of Geosciences in 2020 and M. S. at Key Laboratory of Advanced Energy Materials Chemistry (KLAEMC, Ministry of Education) Nankai University in June of 2023. Her research focuses on electrode materials for Na/K-ion batteries and solid-state Li batteries.

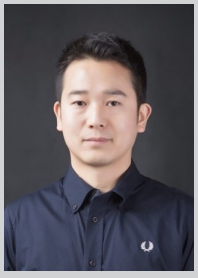

Shizhao Xiong is currently a researcher in Department of Physics at Chalmers University of Technology. He has worked as a postdoc in Chalmers University of Technology from 2019 to 2021. His research interests are focused on understanding of interface evolution in battery systems by using multiphysics simulation and synchrotron-based operando techniques. His interest also covers materials design for next generation batteries, including Li-S batteries, Li metal batteries and solid-state Li batteries.

Fujun Li is a Professor at Key Laboratory of Advanced Energy Materials Chemistry (Ministry of Education), Nankai University. He obtained his Ph.D. degree from the University of Hong Kong in 2011, and then worked as a postdoc fellow at the University of Tokyo and National Institute of Advanced Industrial Science and Technology (Tsukuba), Japan until August of 2015. His research interests include energy materials chemistry, Na (Li)-ion batteries, and Li–O_2 (air) batteries.

Aleksandar Matic is a professor of Physics and Head of the Division for Materials Physics, Department of Physics at Chalmers University of Technology. His research interests span from fundamentals of soft matter to applied research on materials for energy applications. A particular focus is materials for next generation batteries, e.g., Li-S batteries, nanostructured carbon materials, Li-metal anodes and interface engineering of Li-metal surfaces and ionic-liquid based electrolytes.

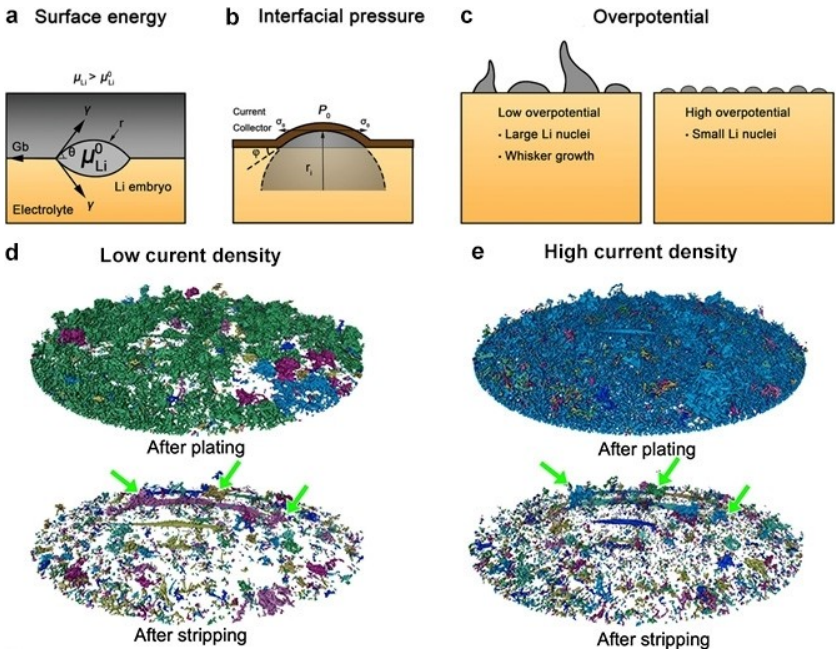

Figure 1. a–c) The progress of Li nucleation and Li whisker growth. Reproduced with permission from Ref. [29] Copyright (2021) Wiley. d, e) The Li plating/stripping morphology at low/high current density. Reproduced with permission from Ref. [20] Copyright (2023) The Authors.

even more complex situation can be expected for SSEs bringing challenges for inhibiting Li dendrite formation and propagation.[27]

2.3. Growth of Li dendrites

In SSLMBs the growth and propagation of Li dendrites are directly influenced by the properties of the SSEs and the SSE/Li-metal interface, e.g., mechanical modulus of the SSE, crystallinity, cracks/defects and their distribution, or voids/porosity at the interface. Monroe and Newman have suggested that SSEs with high shear modulus can suppress the growth of Li dendrite during Li plating.[32,33] Especially, garnet-$Li_7La_3Zr_2O_{12}$ (LLZO) is a type of potential SSEs, due to its high elastic and shear moduli.[17] However, garnet-SSEs still suffer from low CCD, which leads to Li deposition and growth of Li dendrites at low current density, finally causing electric failure.[34] This points to that a high shear modulus alone is not sufficient to suppress of Li dendrite formation and propagation.

Wang et al. have demonstrated that a high electronic conductivity of the SSEs promotes the formation of Li dendrites, since it allows for reduction of Li^+ and formation of Li metal in the bulk of the SSE when the potential reaches the Li-plating potential.[35] Sakamoto et al. first observed that Li preferentially deposits along grain boundaries (GBs) and propagates through the SSE, via SEM, energy dispersive spectrometer (EDS), and auger electron spectroscopy (AES) experiments[36] (Figure 2a). This revealed the crucial role of GBs in the formation of Li dendrites in SSEs. They associated a decreased bad gap in GBs to the reduction of Li ions and formation of local Li filaments at GBs.[37] This was supported by Pan et al. who pointed to a high electronic conductivity of GBs as the main cause of low CCD and metallic Li deposition inside SSEs.[38] Also, the ionic conductivity is central and Islam et al. proposed two types of Li^+ conduction pathways in SSEs, the "granular" pathway and the "GB" pathway. Along the "granular" pathway (Figure 2b) Li ions diffuse through the grains and GBs, and it dominates when the GBs are more resistive than the bulk crystalline structure, for example in the case of Li_3OCl. The "GB" pathway (Figure 2c) will dominate when the conduction of GB is similar to that of the bulk, which is the case of sulfides and some oxide SSEs.[39] Furthermore, Siegel et al. have proposed that the elastic properties of GBs play a role. In general, they are less rigid allowing easier propagation of Li filaments through GBs compared to the stronger bulk SSE.[40]

Pre-existing cracks also play a critical role in the propagation of Li dendrites through an SSE. Figures 2(d, e) illustrates this, where after Li deposition on the surface of the SSE, Li deposition continuously propagates laterally from the initially deposited sites.[26] Cracking/surface degradation of the SSE was not observed, and no short circuit occurred in this experiment (Figure 2d). Nevertheless, when placing the electrode close to the pre-cracked area, Li accumulation was not observed on SSE at the unchanged current density (Figure 2e), instead of which, cracks are filled with Li metal. Moreover, the nature of Li plating depends on surface defects, such as pores, voids, or cracks, at the interface between the SSE and the substrate for deposition. Li deposition will preferentially occur at the defects due to a lower overpotential and electric field concentration (Figure 2d).[26] As soon as the defect is completely filled by deposited Li metal, mechanical stresses within the SSEs tend to increase and form cracks in the bulk as Li metal continues to plate (Figure 2e).[26,41] Therefore, there exists synergistic interplay

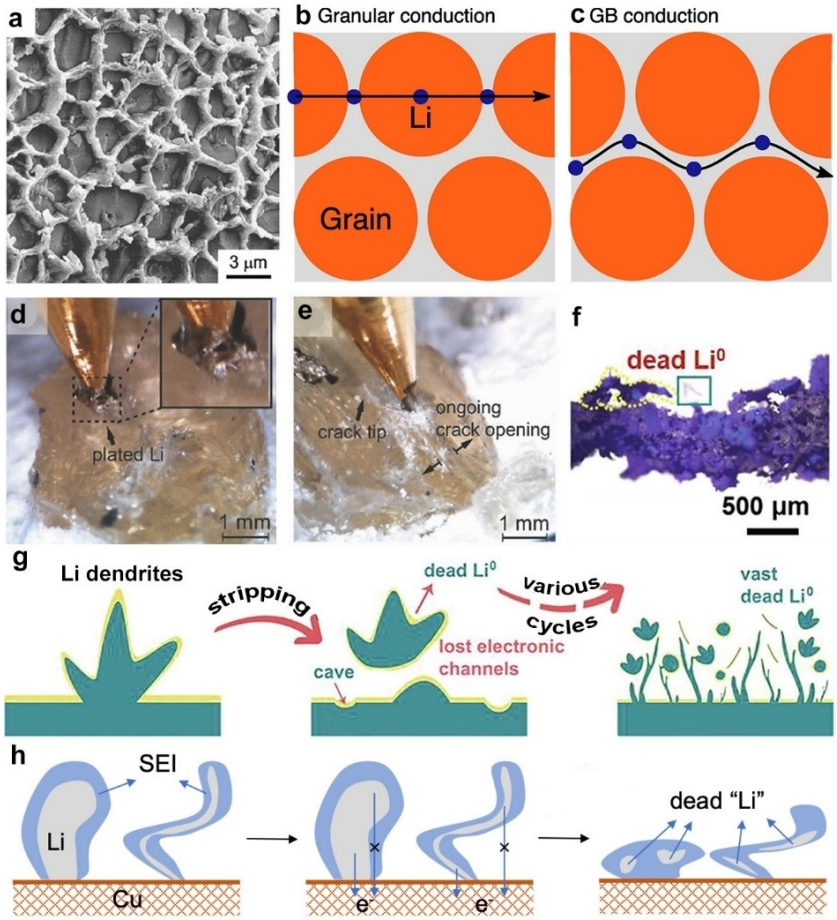

Figure 2. a) The SEM image of Li deposits along GBs. Reproduced with permission from Ref. [36] Copyright (2017) Elsevier. Schematic of b) the "granular" pathway and c) the "GB" pathway. Reproduced with permission from Ref. [39] Copyright (2018) American Chemical Society. d) Li deposition at a pristine as-fractured surface, where surface deposition of Li metal without crack formation or propagation is observed. e) Li deposition at a pre-cracked region, where no surface deposition of Li is observed, whereas growth of a crack from the initially damaged region is observed. Reproduced with permission from Ref. [26] Copyright (2017) Wiley-VCH. f) The SEM image of "dead Li"; g) The scheme of dead Li^0 formation during Li stripping process. Reproduced with permission from Ref. [43] Copyright (2020) Elsevier. h) The diagram of inactive Li generation due to the fast formation of SEI.

between cracks and Li dendrites, namely, on one hand, cracks provide preferential deposition sites for Li, and on the other hand, Li deposition and development of Li dendrites promote the propagation of cracks. External pressure is an important parameter in this context as it can directly influence Li dendrites as well by preventing the progress of electroplating of Li. A higher external pressure generally results in smoother and denser morphology of plated Li and increases the mechanical stability.[42]

2.4. Formation of inactive Li

In addition to the short circuits caused by propagation of Li dendrites through the SSE, the transformation from active Li to inactive Li is another cause of electric failure, leading to capacity fade and decreased Coulombic efficiency (CE) during cycling. The formation of a solid electrolyte interphase (SEI) on the anode consumes active Li during cycling, which decreases the CE. Furthermore, inactive Li could form when metallic Li is wrapped in SEI, or metallic Li which has penetrated into the SSE, losing electric contact due to mechanical stresses or the fragility of formed Li structures, in particular at fast stripping (high discharge rate) or fast formation of SEI (Figure 2g, h).[18,20] This type of inactive Li could also be called "dead Li" (Figure 2f, g), which not only aggravates the diffusion barrier of Li ions and accounts for the high overpotential but also brings about low CE as well as rapid capacity fade.[43]

3. (Electro)chemical Failure

The (electro)chemical failure of SSEs mainly originates from the formation of an unstable interphase between SSEs and Li metal anode. An unstable interphase promotes a continuous decomposition of the SSE and accumulation of side-reaction products, leading to increased impedance and contact loss, accelerating (electro)chemical failure.

3.1. Formation of interphase

The interphase formed between SSEs and Li metal anode due to the reduction of the SSE can be classified into three types: kinetically stable interphase (KSI), mixed conductive interphase (MCI), and stable SEI. Firstly, in the case of KSI (Figure 3a), the SSE is reduced spontaneously, and the formed interphase is electronically insulating. The electrochemical potential of Li decreases across the interphase from the Li anode to SSE, to be within the electrochemical window of the SSE due to the poor electronic conductivity of the interphase. In this situation, the decomposition of the SSE has no thermodynamic driving force to continue, and it is protected from continuous reduction.[44,45] In contrast, the reduction of SSE in the case of forming MCI is at the same time, but the interphase is both electron and ion conductive, facilitating the further reduction of the SSE.[45] Therefore, the continuous growth of the interphase occurs also leading to a volume change which is detrimental to interphase stability. Moreover, MCI is predicted to grow rapidly at high current density leading to higher pressure (large volume change) and acceleration of the degradation of the SSE. Thirdly, in SEI, SSEs are stable with Li-metal anodes due to the electron insulative and ion conductive of SEI (Figure 3c).[12]

The type of formed interphase between an SSE and Li metal anode depends on the chemical composition of the SSE. SSEs without transition metals, such as LiPON and $Li_7P_3S_{11}$ are kinetically stable towards Li metal anodes. The in-situ formed binary Li compounds, such as LiF, LiCl, LiBr, Li_2O, Li_2S, LiH, or Li_3N, form an interphase that is thermodynamically stable and passivates the SSE from continuous reduction. However, the ionic conductivity of interphase created by compounds is usually low, increasing the impedance of the cell and impeding the electrochemical reduction of Li^+.[46] Moreover, KSI is formed on the surface of garnet and perovskite-type SSEs since the transition metal in garnet and perovskite type structures are difficult to reduce to a conductive metallic state. An electronically insulating layer will be obtained which inhibits the continuous reduction of the SSE. Most inorganic SSEs, such as $Li_{10}GeP_2S_{12}$ (LGPS) and $Li_{1+x}Al_xTi_{2-x}(PO_4)_3$ (LATP) form an MCI at the Li/SSEs interface. The instability is mainly associated to the high-valence cations (e.g., P^{5+}, Ge^{4+}, Ta^{5+}, Ti^{4+}, and In^{3+}), which can be reduced to an electron-conductive metallic state. The persistent reduction of the SSE is facilitated by the electronically conductive interphase, ultimately leading to (electro)chemical failure of the SSMB.[45]

A specific example is the formation of different interphases from two types of SSEs, $Li_{10}SnP_2S_{12}$ (LSPS) and Li_6PS_5Cl (LPSC), which is also beneficial to build a deeper understanding of the influence of stack pressure and the processing of electrolyte. In the case of LSPS, an MCI forms, and continuously grows, at the interface of Li/SSE without the formation of Li filaments.[47,48] On the other hand, a thinner interphase with the ability to self-passivate is formed on the surface of LPSC resulting from its electronically insulating nature, but at the same time, non-uniform Li plating occurs. This contrasting behavior is related to the pressure built up during continuous SEI growth that leads to an increased stack pressure in LPSC-based cells. Sakamoto et al. also proposed that a current-dependent "critical stack pressure" will lead to significant polarization during electrochemical cycling.[49]

3.2. Decomposition of SSEs

In addition to the formation of Li/SSEs interphase, SSEs suffer from decomposition when the operating voltage is outside their electrochemical stability window. Unfortunately, the electrochemical stability windows of most sulfides and garnets are very narrow, such as LGPS, which is restricted to 1.7–2.4 V.[50] Zhang and colleagues further investigated the decomposition processes and products formed under different voltage windows with $Li_7P_3S_{11}$ (LPS). The results indicated that using a wide electrochemical window, LPS suffered a severe redox reaction of leading to the accumulation of the decomposition products, such as Li_2S, the amount of which increased with the voltage window.[51] Adams and coworkers also explored the decomposition behavior of LAGP by electrochemical cycling tests and first-principles calculations.[22] The increased electronical conductivity of voids or GBs in LAGP promotes the decomposition and the formation of $Li_4P_2O_7$, Li_3PO_4, $Ge_5P_6O_{25}$, $AlPO_4$, and GeO. Finite element method simulations clarified that the accumulation of deposition products leads to a peak of internal stress of 2.5–125 GPa relevant to various Li excess ratios (0 to 6), which subsequently causes volume expansion. This value exceeds the critical failure stress of LAGP and leads to crack formation after several cycles.[22] As a result, interfacial polar-

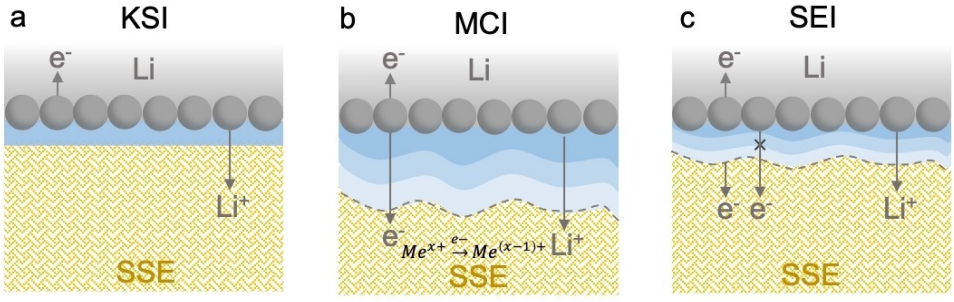

Figure 3. Interphase growth between the Li metal and different SEs, a) kinetically stable interphase (KSI); b) mixed conductive interphase (MCI); c) solid electrolyte interphase (SEI).

ization and cell resistance increase, with fast capacity degradation and (electro)chemical failure as a result.

4. Mechanical Failure

4.1. Origin of mechanical failure

The mechanical failure of SSEs mainly results from crack infiltration, interface delamination, and void/pore formation, which, on one hand, promote Li dendrite propagation eventually causing short circuit, on the other hand, cause contact loss increasing the overpotential and resulting in capacity decay.[52] The process of crack formation and interface delamination occurs as follows. Nonuniform Li deposition leads to severe fluctuation of the Li/SSEs interfaces due to the rigidity of SSEs compared to liquid electrolytes. The fluctuating interfaces lead to void formation or disconnection with contact loss or delamination. This type of interface degradation impedes the Li-ion transport with increasing interfacial impedance and capacity decay. Furthermore, the rigid SSE cannot accommodate the volume change which generates large and nonuniform distribution of stresses, resulting in mechanical damage to the interface. After repetitive cycles, significant interphase bending or microcracking occurs, which accumulates to form macroscopic cracks and loss of grain contact and connectivity, thus increasing polarization and leading to capacity losses (Figure 4a).[50,53] As a result, the as-generated and as well as pre-existing defects act as the preferential Li deposition sites promoting the Li dendrites infiltration.[50]

Mechanical failure is affected by several factors, such as nature of Li deposition, current density, stress release, physicochemical properties of the SSE, or defect distribution. Li deposition and the cracking processes give an electro-chemical-mechanical coupled effect. The formed cracks, voids, and primary defects lead to uneven distribution of overpotential, and Li is preferentially deposited at sites with low overpotential. The presence of these sites leads to further selective deposition of Li and the formation of Li filaments. Stress will accumulate at the tip of Li filaments, pushing the Li filament into the SSE and further accelerating SSE failure. A simplified geometry of a Li filament based on a typical inorganic SSE is shown in Figure 4(b) with the pressure from the Li metal indicated. The model shows that maximum stresses are found at the filament tip.[26] High electron conductivity of the Li filament contributes to the further deposition of Li and leads to greater overpotential, widening and lengthening of these structures. The changes in stress distribution due to Li dendrite propagation accelerates crack infiltration.[50] This can lead to different morphology/geometries of deposited Li (for example, "straight", "spalling", "branching", and "diffuse" types) created inside cracks.[23] This Li filament geometry together with applied current density are crucial factors to determine the propagation rate of Li dendrites and the failure time of SSLMBs by internal short circuits. It is found that a stress-field integrated network is easily formed between adjacent filaments when they have small

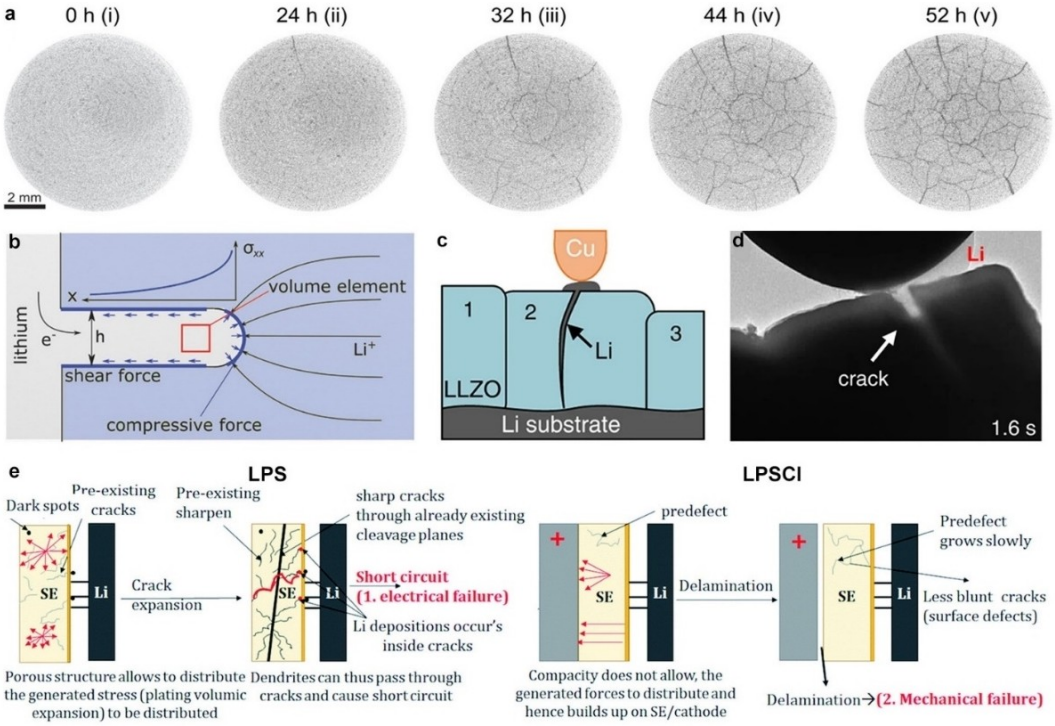

Figure 4. a) The formation progress of cracks in SSE pellet. Reproduced with permission from Ref. [53] Copyright (2019) American Chemical Society. b) Simplified schematic of a Li filament in SSE matrix. Reproduced with permission from Ref. [26] Copyright (2017) Wiley. c) Li eruption at the interface to crack a single LLZO particle; d) Schematic illustration of crack opening and Li filling in SSE. Reproduced with permission from Ref. [16] Copyright (2022) Springer Nature. e) Schematic summarizing all the observed failure modes observed in the LPS vs. LPSCI SSEs. Reproduced with permission from Ref. [15] Copyright (2022) Royal Society of Chemistry.

diameters and high number density, with a fast development of the damage in the SSE.

4.2. Crack formation

The relationship between cracks and Li dendrite propagation was investigated by in-situ X-ray CT based on the Li/Li_6PS_5Cl (LPSC)/Li cell by Bruce and coworkers.[19] During plating, cracking starts with conical "pothole"-like cracks (spallation) at the interface with the Li electrode where plating occurs. Subsequently, cracks propagation initiates from the spallation located at the plated Li electrode and reaches the other electrode where stripping occurs resulting in transverse cracks across the LPSC-SSE. The formation and development of the cracks are driven by the growth of Li via broadening the pathway, leading to the penetration of cracks through the entire SSE ahead of the connection of the two electrodes by Li.[19] Shearing et al. explored the order of crack formation and Li dendrite propagation by tracking Li penetration in SSEs by in-situ synchrotron X-ray CT. The results indicate that crack infiltration is much faster than Li growth so that a large number of cracks near the cathode side are empty and the cell operates normally. The deposited Li after short circuit (cell failure) was segmented, and its distribution was visualized.[54] The cracks travel ahead of Li dendrites, and cracks in turn serve as the propagation route for Li dendrites, ultimately causing short circuits. Li dendrite propagation and cracks infiltration promote each other leading to an enhancement of the processes. Furthermore, Chueh et al. proposed that nanoscale cracks and current focusing are the main cause of Li intrusion into SSEs rather than electrochemical reduction.[55]

Wang et al. revealed that the initiation of cracks at the Li/SSE interface depends on the local current density and mechanism of mass/stress release.[16] They investigated the Li deposition dynamics and associated failure mechanism of SSEs by visualizing the interphase evolution of Li/$Li_7La_3Zr_2O_{12}$ (LLZO) through in situ TEM. Li propagated laterally on LLZO facilitated by the stress resulting from the Li deposition, the strong mechanical pressure and low current density. After Li "eruption", the LLZO-SSE will be cracked without defects due to the blowout of the local stress as high as the GPa level (Figure 4c, d).

Intrinsic physicochemical properties of SSEs affect the process of mechanical failure as well, and Davoisne et al. studied this influence based on two sulfide-based SSEs, β-Li_3PS_4 (LPS) and Li_6PS_5Cl (LPSCl).[15] LPSCl inhibits dendrite propagation to a larger degree, due to a higher compactness of LPSCl compared to LPS, in the case of which, the cathode near the side of SSE delaminates because the formed electro-chemo-mechanical stress is exerted upon the cathode. LPS has higher porosity, which leads to faster crack growth, since Li deposits inside these pores at the anode interface, causing mechanical stress on the SSE and elongation of neighboring pre-existing cracks. Both of these two SSEs display mechanical failure after cycling, in LPSCl it tends to occur through delamination in the cathode whereas in LPS it is preferential due to cracking due the different flexibility and porosity (Figure 4e).

4.3. Formation of pores and voids

The interfacial and internal defects and voids of SSEs also induces nonuniform electrodeposition of Li and trigger mechanical degradation of SSEs.[52] Liu et al. built a modified electro-chemo-mechanical model to describe the interplay of interfacial and internal defects on mechanical failure, which provides the relationship between mechanical failure of SSEs and electrodeposition of Li metal.[23] Stress transmits through the SSE due to Li deposition at the Li/SSE interface, thus generating damage inside the SSE, which is governed by the morphology of interfacial defects. Damage becomes more drastic if there exist defects with sharper angles (cube) or larger fluctuation at the contact area (semi-ellipse) (Figure 5a). Small-sized semispherical interface defects lead to smaller cracks within the SSE (Figure 5b), and with the expansion of the semi-sphere radius the cracks grow wider and longer. Furthermore, the transmission of generated stress in the SSE is also influenced by internal voids, which functions as hubs for regulating damage processes and govern the mechanical failure of SSEs (Figure 5c). The larger number of internal voids lead to the shorter damaging time, and the shorter distance between internal voids also shortens the damage time.[52]

The formation of voids/pores is another source of mechanical failure. Voids form in the Li anode at the surface when the stripping current density removes Li from the interface faster than it can be replenished, which leads to contact loss, increased impedance, and locally increased current density, promoting formation of Li dendrites.[6] The size of voids in an SSE pellet less affects the failure process compared to the number of voids. Therefore, decreasing the porosity of SSE has been considered as an effective strategy to suppress SSE failure.[23]

Zhao et al. proposed a mechanical model for predicting the void evolution during cycling, the results of which indicate that void geometry is highly related to the charge/discharge rate.[24] As shown in Figure 5(d), the void expands along the interface due to the stripping currents, while Li plating transforms to the contraction of the void edges, giving rise to complete void occlusion. Some voids are eliminated during plating, while the occluded voids will reopen in the subsequent stripping process, causing accumulation of voids and increased loss of contact.[24] A higher applied current density will enhance these phenomena. The local current density and stripping polarization increase at the void edges, which results in Li dendrite formation during plating.[24] The number of voids/pores is reduced with the application of mechanical pressure, increasing the electric contact between the electrode and SSE. Smaller voids can finally be eliminated if the pressure is large enough. McDowell et al. investigated the influence of local interfacial roughness on formation of voids during Li stripping by using operando synchrotron X-ray CT to probe the evolution of Li/SSE interfaces during battery cycling.[56] The results show that the

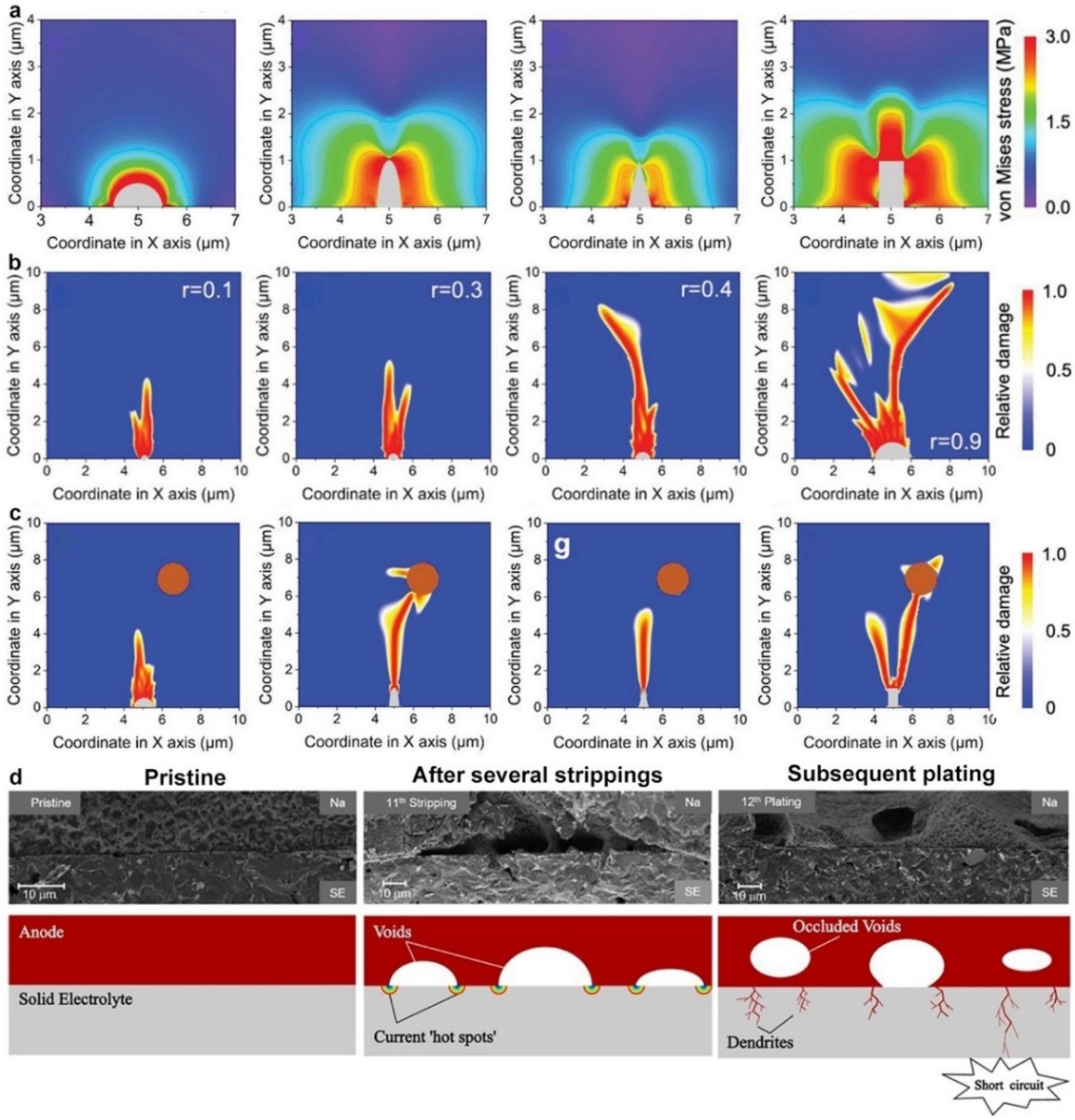

Figure 5. a) Visualization of von Mises stress caused by the electrodeposition of Li at the interface of SSEs. b) Visualization of the corresponding damage region in the SSEs with various radius. c) Visualization of damage region with various interfacial defects. Reproduced with permission from Ref. [52] Copyright (2023) Wiley. Interplay between voiding and dendrite formation: SEM images and sketches of the process of voiding and dendrite formation during plating and stripping cycles. Reproduced with permission from Ref. [24] Copyright (2022) Elsevier.

tendency to form voids is increasing with increased local interfacial roughness, and the local compression caused by the growth of the interphase may close the formed voids. The reduction process is also observed to form voids because the Li metal anode is consumed and leaving voids due to a chemical side reaction.

5. Conclusions and Future Prospects

The failure of SSEs is influenced by various factors, including the properties of the formed SSEs/Li interphase, physicochemical properties of SSEs (e.g., surface defects and crystalline structure), external conditions (e.g., current density and cell pressure), and intrinsic mechanical properties of SSEs. Based on the various mechanisms, the failure of SSEs can be classified as electric, (electro)chemical, and mechanical failure. The failure mechanisms of SSEs cannot be studied individually, due to their intimate relationship and coupling. Thus, the systematic understanding on the coupled electric-(electro)chemical-mechanical failure mechanisms of SSEs is still not well developed, which is important to advance research and development of SSEs.

The uneven deposition of Li is the main reason for the growth of Li dendrites. Li preferentially deposits on surface defects and initial nucelli, and Li filament propagation along GBs and further across the SSE leads to short circuit and cell failure. The side reactions between SSEs and Li electrodes form an unstable interphase due to the (electro)chemical instability

Table 1. Strategies to address the failure of SSEs.

Strategies		Functions		
Structure design	3D Li anode[34]	Inhibit dendrite growth	Buffer volume change	
	Carbon composite materials[42]	Homogenous Li deposition	Buffer volume change	
	Composite electrolyte[57]	Increase ion conductivity	Buffer volume change	Inhibit dendrite growth
Additives	Organic electrolytes[58]	Interface wetting and isolation	Prevent SSE reduction	
	Functional additives[59]	Mechanically robust interface	Inhibit dendrite growth	Decrease interface resistance
Interface design	Inorganic coating[60]	Inhibit dendrite growth	Prevent side reactions	Buffer volume change
	Polymer coating[61]	Increase interface contact area	Inhibit dendrite growth	

of most SSEs towards Li metal. This kinetically and/or thermodynamically unstable interphase accelerates the nonuniform deposition of Li and Li dendrite propagation, and the continuous decomposition of SSEs increases the impedance of the cell when exceeding the electrochemical stability window, both of which degrade battery capacity and cause cell (electro)chemical failure. Moreover, cracking and pulverization occur due to the local increased stress induced by the inevitable volume expansion and interface fluctuations during repeated Li plating/stripping, which lead to contact loss and promote the propagation of Li dendrites, thus degrading the electrochemical performance of cell.

To address the electro-chemo-mechanical failure of SSEs, various strategies have been developed, as listed in Table 1. Structure design of anode and electrolyte, addition of organic electrolytes, and design of artificial interface are the main strategies are explored to prevent the failure of SSEs, and their functions include suppressing Li dendrite growth, regulating Li deposition and wetting interface. Despite the significant achievements in this field, the understanding of SSE failure is still not comprehensive enough. To facilitate the practical application of SSLMBs in the future, great efforts should be devoted to investigating SSE failure. It is necessary to overall consider the three types of SSEs failure mechanisms and establish a comprehensive evaluation model based on experiments and theoretical analysis, thereby improving the electrochemical performance of SSLMBs for practical use. Additionally, advanced characterization tools, including electrochemical testing, *operando* X-ray techniques, and in situ electron microscopy, should be developed to detect and track the growth of Li dendrites, voids/pores formation, cracking progress, interphase evolution, cell pressure change, and electrochemical signal response from multi-dimensions. Furthermore, building a diagnostic system to prevent thermal runaway and cell failure is significant for the improvement of safety. Based on the full-scale investigation of SSE failure, a systematic and comprehensive understanding could be attained, providing insights for the design and development of SSEs with high energy density, safety, and cycling stability.

Acknowledgements

Q. W. and F. L. thank for the financial support from the National Natural Science Foundation of China (Grant No. 52171215). S. X. and A. M. acknowledge the support from Chalmers Areas of Advance Materials Science and Energy, Batteries Sweden (BASE) and Energimyndigheten.

Conflict of Interests

The authors declare no conflict of interest.

Data Availability Statement

The data that support the findings of this study are available from the corresponding author upon reasonable request.

Keywords: solid-state electrolyte · lithium-metal anode · electric failure · (electro)chemical failure · mechanical failure

[1] J. Geng, Y. Ni, Z. Zhu, Q. Wu, S. Gao, W. Hua, S. Indris, J. Chen, F. Li, *J. Am. Chem. Soc.* **2023**, *145*, 1564–1571.
[2] M. Pasta, D. Armstrong, Z. L. Brown, J. Bu, M. R. Castell, P. Chen, A. Cocks, S. A. Corr, E. J. Cussen, E. Darnbrough, V. Deshpande, C. Doerrer, M. S. Dyer, H. El-Shinawi, N. Fleck, P. Grant, G. L. Gregory, C. Grovenor, L. J. Hardwick, J. T. S. Irvine, H. J. Lee, G. Li, E. Liberti, I. McClelland, C. Monroe, P. D. Nellist, P. R. Shearing, E. Shoko, W. Song, D. S. Jolly, C. I. Thomas, S. J. Turrell, M. Vestli, C. K. Williams, Y. Zhou, P. G. Bruce, *J. Phys. E* **2020**, *2*, 032008.
[3] C. Wang, L. Liu, S. Zhao, Y. Liu, Y. Yang, H. Yu, S. Lee, G. H. Lee, Y. M. Kang, R. Liu, F. Li, J. Chen, *Nat. Commun.* **2021**, *12*, 2256.
[4] Y. Su, J. Hao, X. Liu, Y. Yang, *Batteries & Supercaps* **2022**, *6*, e202200359.
[5] X. Ke, Y. Wang, L. Dai, C. Yuan, *Energy Storage Mater.* **2020**, *33*, 309–328.
[6] J. Kasemchainan, S. Zekoll, D. Spencer Jolly, Z. Ning, G. O. Hartley, J. Marrow, P. G. Bruce, *Nat. Mater.* **2019**, *18*, 1105–1111.
[7] M. Balaish, J. C. Gonzalez-Rosillo, K. J. Kim, Y. Zhu, Z. D. Hood, J. L. M. Rupp, *Nat. Energy* **2021**, *6*, 227–239.
[8] M. J. Wang, E. Kazyak, N. P. Dasgupta, J. Sakamoto, *Joule* **2021**, *5*, 1371–1390.
[9] S. Ohno, C. Rosenbach, G. F. Dewald, J. Janek, W. G. Zeier, *Adv. Funct. Mater.* **2021**, *31*, 2010620.
[10] Y. Ren, T. Danner, A. Moy, M. Finsterbusch, T. Hamann, J. Dippell, T. Fuchs, M. Müller, R. Hoft, A. Weber, L. A. Curtiss, P. Zapol, M. Klenk, A. T. Ngo, P. Barai, B. C. Wood, R. Shi, L. F. Wan, T. W. Heo, M. Engels, J. Nanda, F. H. Richter, A. Latz, V. Srinivasan, J. Janek, J. Sakamoto, E. D. Wachsman, D. Fattakhova-Rohlfing, *Adv. Energy Mater.* **2022**, *13*, 2201939.
[11] C. Yuan, W. Lu, J. Xu, *Adv. Energy Mater.* **2021**, *11*, 2101807.

[12] J. Janek, W. G. Zeier, *Nat. Energy* **2023**, *8*, 230–240.
[13] J. A. Lewis, J. Tippens, F. J. Q. Cortes, M. T. McDowell, *Trends Chem.* **2019**, *1*, 845–857.
[14] S. H. Kim, K. Kim, H. Choi, D. Im, S. Heo, H. S. Choi, *J. Mater. Chem. A* **2019**, *7*, 13650–13657.
[15] N. G. Yadav, N. Folastre, M. Bolmont, A. Jamali, M. Morcrette, C. Davoisne, *J. Mater. Chem. A* **2022**, *10*, 17142–17155.
[16] H. Gao, X. Ai, H. Wang, W. Li, P. Wei, Y. Cheng, S. Gui, H. Yang, Y. Yang, M. S. Wang, *Nat. Commun.* **2022**, *13*, 5050.
[17] E. Kazyak, R. Garcia-Mendez, W. S. LePage, A. Sharafi, A. L. Davis, A. J. Sanchez, K.-H. Chen, C. Haslam, J. Sakamoto, N. P. Dasgupta, *Matter* **2020**, *2*, 1025–1048.
[18] C. Fang, J. Li, M. Zhang, Y. Zhang, F. Yang, J. Z. Lee, M. H. Lee, J. Alvarado, M. A. Schroeder, Y. Yang, B. Lu, N. Williams, M. Ceja, L. Yang, M. Cai, J. Gu, K. Xu, X. Wang, Y. S. Meng, *Nature* **2019**, *572*, 511–515.
[19] Z. Ning, D. S. Jolly, G. Li, R. De Meyere, S. D. Pu, Y. Chen, J. Kasemchainan, J. Ihli, C. Gong, B. Liu, D. L. R. Melvin, A. Bonnin, O. Magdysyuk, P. Adamson, G. O. Hartley, C. W. Monroe, T. J. Marrow, P. G. Bruce, *Nat. Mater.* **2021**, *20*, 1121–1129.
[20] M. Sadd, S. Xiong, J. R. Bowen, F. Marone, A. Matic, *Nat. Commun.* **2023**, *14*, 854.
[21] Y. Cheng, L. Zhang, Q. Zhang, J. Li, Y. Tang, C. Delmas, T. Zhu, M. Winter, M.-S. Wang, J. Huang, *Mater. Today* **2021**, *42*, 137–161.
[22] L. He, J. A. S. Oh, K. Watarai, M. Morita, Y. Zhao, Q. Sun, T. Sakamoto, L. Lu, S. Adams, *Chem. Mater.* **2021**, *33*, 6841–6852.
[23] X. Xu, Y. Liu, O. O. Kapitanova, Z. Song, J. Sun, S. Xiong, *Adv. Mater.* **2022**, *34*, e2207232.
[24] Y. Zhao, R. Wang, E. Martínez-Pañeda, *J. Mech. Phys. Solids* **2022**, *167*, 104999.
[25] D. Bistri, A. Afshar, C. V. Di Leo, *Meccanica* **2020**, *56*, 1523–1554.
[26] L. Porz, T. Swamy, B. W. Sheldon, D. Rettenwander, T. Frömling, H. L. Thaman, S. Berendts, R. Uecker, W. C. Carter, Y. M. Chiang, *Adv. Energy Mater.* **2017**, *7*, 1701003.
[27] X. R. Chen, B. C. Zhao, C. Yan, Q. Zhang, *Adv. Mater.* **2021**, *33*, e2004128.
[28] J. A. Lewis, C. Lee, Y. Liu, S. Y. Han, D. Prakash, E. J. Klein, H. W. Lee, M. T. McDowell, *ACS Appl. Mater. Interfaces* **2022**, *14*, 4051–4060.
[29] Y. Lu, C. Z. Zhao, H. Yuan, X. B. Cheng, J. Q. Huang, Q. Zhang, *Adv. Funct. Mater.* **2021**, *31*, 2009925.
[30] Y. Liu, X. Xu, M. Sadd, O. O. Kapitanova, V. A. Krivchenko, J. Ban, J. Wang, X. Jiao, Z. Song, J. Song, S. Xiong, A. Matic, *Adv. Sci.* **2021**, *8*, 2003301.
[31] M. Motoyama, M. Ejiri, Y. Iriyama, *J. Electrochem. Soc.* **2015**, *162*, A7067–A7071.
[32] C. Monroe, J. Newman, *J. Electrochem. Soc.* **2005**, *152*, A396–A404.
[33] C. Monroe, J. Newman, *J. Electrochem. Soc.* **2004**, *151*, A880–A886.
[34] T. Krauskopf, R. Dippel, H. Hartmann, K. Peppler, B. Mogwitz, F. H. Richter, W. G. Zeier, J. Janek, *Joule* **2019**, *3*, 2030–2049.
[35] F. Han, A. S. Westover, J. Yue, X. Fan, F. Wang, M. Chi, D. N. Leonard, N. J. Dudney, H. Wang, C. Wang, *Nat. Energy* **2019**, *4*, 187–196.
[36] E. J. Cheng, A. Sharafi, J. Sakamoto, *Electrochim. Acta* **2017**, *223*, 85–91.
[37] X. Liu, R. Garcia-Mendez, A. R. Lupini, Y. Cheng, Z. D. Hood, F. Han, A. Sharafi, J. C. Idrobo, N. J. Dudney, C. Wang, C. Ma, J. Sakamoto, M. Chi, *Nat. Mater.* **2021**, *20*, 1485–1490.
[38] Y. Song, L. Yang, W. Zhao, Z. Wang, Y. Zhao, Z. Wang, Q. Zhao, H. Liu, F. Pan, *Adv. Energy Mater.* **2019**, *9*, 1900671.
[39] J. A. Dawson, P. Canepa, T. Famprikis, C. Masquelier, M. S. Islam, *J. Am. Chem. Soc.* **2018**, *140*, 362–368.
[40] S. Yu, D. J. Siegel, *ACS Appl. Mater. Interfaces* **2018**, *10*, 38151–38158.
[41] Y. Liu, X. Xu, X. Jiao, O. O. Kapitanova, Z. Song, S. Xiong, *Adv. Mater.* **2023**, *8*, 2301152.
[42] X. Shen, R. Zhang, P. Shi, X. Chen, Q. Zhang, *Adv. Energy Mater.* **2021**, *11*, 2003416.
[43] X.-R. Chen, C. Yan, J.-F. Ding, H.-J. Peng, Q. Zhang, *J. Energy Chem.* **2021**, *62*, 289–294.
[44] Y. Zhu, X. He, Y. Mo, *ACS Appl. Mater. Interfaces* **2015**, *7*, 23685–23693.
[45] Z. Tong, S. B. Wang, Y. K. Liao, S. F. Hu, R. S. Liu, *ACS Appl. Mater. Interfaces* **2020**, *12*, 47181–47196.
[46] X. Miao, S. Guan, C. Ma, L. Li, C. W. Nan, *Adv. Mater.* **2023**, 2206402. https://doi.org/10.1002/adma.202206402.
[47] C. Lee, S. Y. Han, J. A. Lewis, P. P. Shetty, D. Yeh, Y. Liu, E. Klein, H.-W. Lee, M. T. McDowell, *ACS Energy Lett.* **2021**, *6*, 3261–3269.
[48] R. Koerver, W. Zhang, L. de Biasi, S. Schweidler, A. O. Kondrakov, S. Kolling, T. Brezesinski, P. Hartmann, W. G. Zeier, J. Janek, *Energy Environ. Sci.* **2018**, *11*, 2142–2158.
[49] M. J. Wang, R. Choudhury, J. Sakamoto, *Joule* **2019**, *3*, 2165–2178.
[50] J. Liu, H. Yuan, H. Liu, C. Z. Zhao, Y. Lu, X. B. Cheng, J. Q. Huang, Q. Zhang, *Adv. Energy Mater.* **2021**, *12*, 2100748.
[51] G.-L. Zhu, C.-Z. Zhao, H. Yuan, B.-C. Zhao, L.-P. Hou, X.-B. Cheng, H.-X. Nan, Y. Lu, J. Zhang, J.-Q. Huang, Q.-B. Liu, C.-X. He, Q. Zhang, *Energy Storage Mater.* **2020**, *31*, 267–273.
[52] S. Xiong, X. Xu, X. Jiao, Y. Wang, O. O. Kapitanova, Z. Song, Y. Liu, *Adv. Energy Mater.* **2023**, *13*, 2203614.
[53] J. Tippens, J. C. Miers, A. Afshar, J. A. Lewis, F. J. Q. Cortes, H. Qiao, T. S. Marchese, C. V. Di Leo, C. Saldana, M. T. McDowell, *ACS Energy Lett.* **2019**, *4*, 1475–1483.
[54] S. Hao, S. R. Daemi, T. M. M. Heenan, W. Du, C. Tan, M. Storm, C. Rau, D. J. L. Brett, P. R. Shearing, *Nano Energy* **2021**, *82*, 105744.
[55] G. McConohy, X. Xu, T. Cui, E. Barks, S. Wang, E. Kaeli, C. Melamed, X. W. Gu, W. C. Chueh, *Nat. Energy* **2023**, *8*, 241–250.
[56] J. A. Lewis, F. J. Q. Cortes, Y. Liu, J. C. Miers, A. Verma, B. S. Vishnugopi, J. Tippens, D. Prakash, T. S. Marchese, S. Y. Han, C. Lee, P. P. Shetty, H. W. Lee, P. Shevchenko, F. De Carlo, C. Saldana, P. P. Mukherjee, M. T. McDowell, *Nat. Mater.* **2021**, *20*, 503–510.
[57] W. Zhang, J. Nie, F. Li, Z. Wang, C. Wang, *Nano Energy* **2018**, *45*, 413–419.
[58] Z. Zhang, S. Chen, J. Yang, J. Wang, L. Yao, X. Yao, P. Cui, X. Xu, *ACS Appl. Mater. Interfaces* **2018**, *10*, 2555–2565.
[59] B. Xu, H. Duan, H. Liu, C. Wang, S. Zhong, *ACS Appl. Mater. Interfaces* **2017**, *9*, 21077–21082.
[60] X. Han, Y. Gong, K. Fu, X. He, G. Hitz, J. Dai, A. Pearse, B. Liu, H. Wang, G. Rubloff, Y. Mo, V. Thangadurai, E. Wachsman, L. Hu, *Nat. Mater.* **2017**, *16*, 572–579.
[61] X.-X. Zeng, Y.-X. Yin, Y. Shi, X.-D. Zhang, H.-R. Yao, R. Wen, X.-W. Wu, Y.-G. Guo, *Chem* **2018**, *4*, 298–307.

Manuscript received: July 19, 2023
Revised manuscript received: September 3, 2023
Accepted manuscript online: September 4, 2023
Version of record online: September 21, 2023